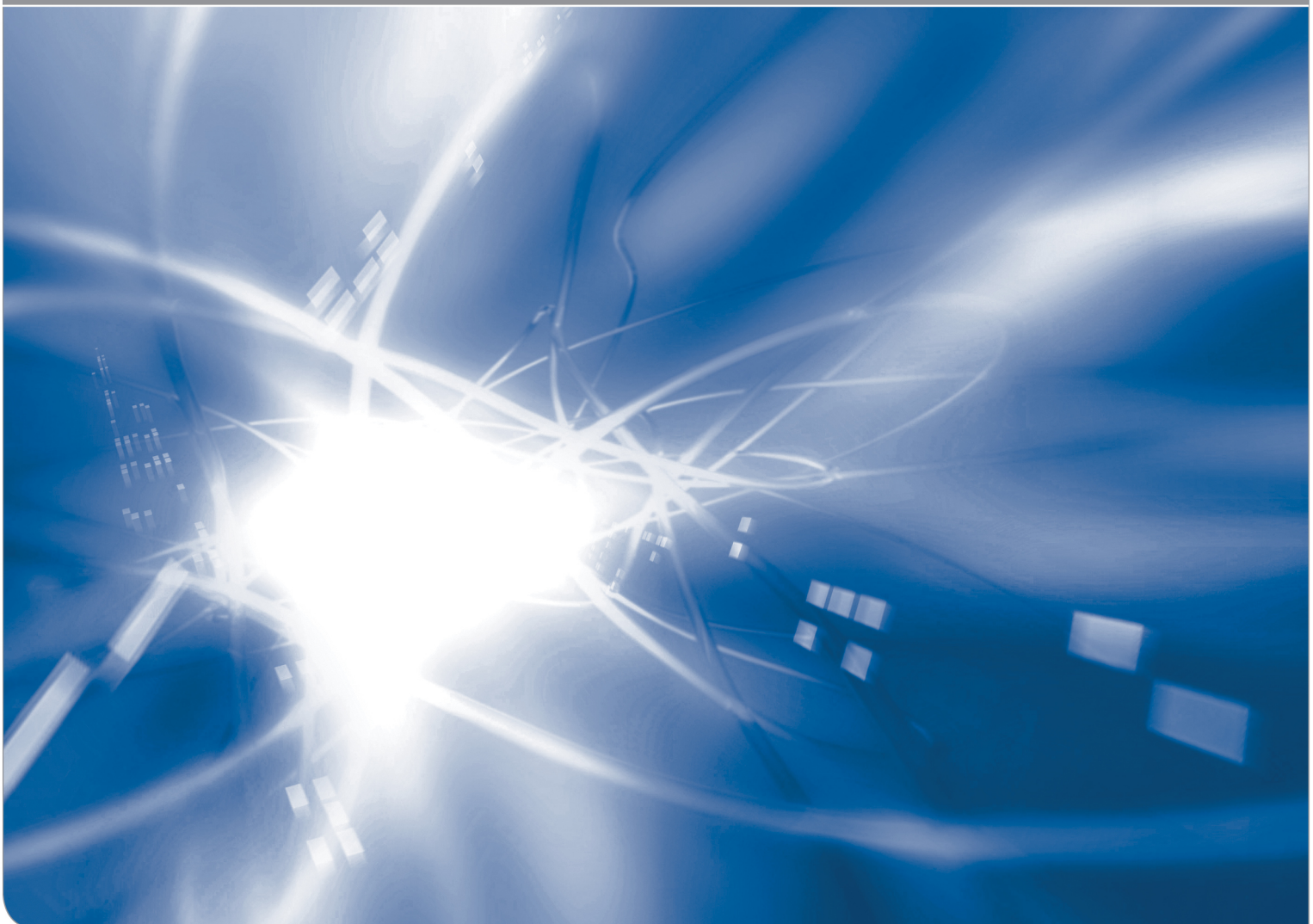


Evaluation of crack profiles by Bando et al. Analysis of crack opening displacements

T. Fett, K.G. Schell, G. Rizzi

KIT SCIENTIFIC WORKING PAPERS **110**



IAM Institute for Applied Materials

Impressum

Karlsruher Institut für Technologie (KIT)
www.kit.edu



This document is licensed under the Creative Commons Attribution – Share Alike 4.0 International License (CC BY-SA 4.0): <https://creativecommons.org/licenses/by-sa/4.0/deed.en>

2019

ISSN: 2194-1629

Abstract

The behavior of cracks in glass is discussed contrary for many years. Both purely elastic material behavior as well as plasticity and viscosity were discussed. One of the key results were the crack opening measurements of Bando which were considered for an indication of non-elastic behavior.

There are two effects of water, damage by breaking the ring structure due to chemical water reaction and swelling. In this short note, the effect of damage by the water-glass reaction is addressed. In this report we deal with a purely linear attempt by the J-integral.

Contents

1	Experimental observation	1
2	Theoretical consequences	4
	2.1 Conclusions on the basis of the J-Integral	4
	2.2 Estimation of crack opening displacements (COD)	5
3	Limit case estimation of zone sizes	7
	References	9

1. Experimental observation

Since many years, the deformation behaviour at crack tips in silica is discussed controversially. On the one hand, the behavior is described purely elastic. On the other hand, plastic and viscous behavior is assumed. As an argument for the second interpretation the crack opening behaviour measured by Bando et al. [1] on thin lamellas is given. In their paper the authors show COD-profiles of cracks under load which were produced in thin silica sheets of 20-40nm thickness.

Two of the images by Bando et al. [1] show cracks which were damaged in air and rather rapidly transferred into the TEM-device. These profiles are re-plotted in Fig. 1a.

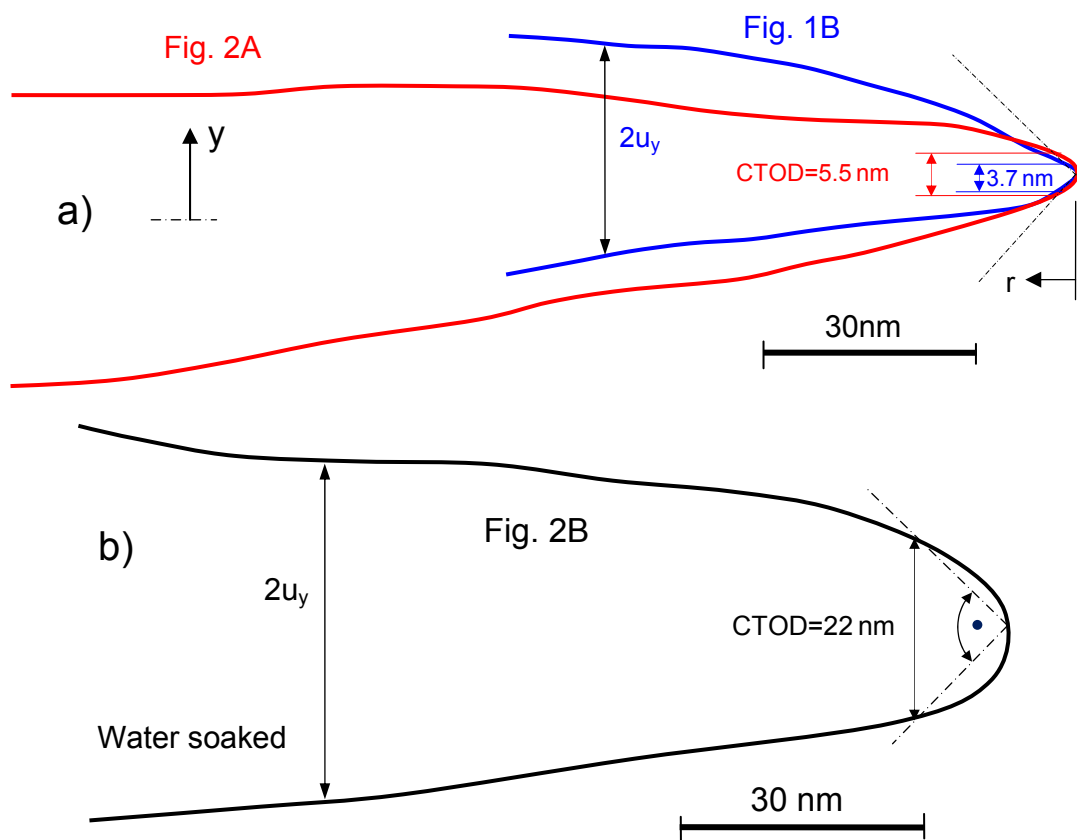


Fig. 1 a) COD profiles for the two cracks generated in normal lab air according to Figs. 1B (blue profile) and 2A (red profile) of [1], b) profile for long-time water-soaked specimen, Fig. 2B.

The opening at the tip of the physical crack, called *Crack Tip Opening Displacement* (CTOD), δ_t , is in fracture mechanics defined as twice the COD in a distance of $r = \frac{1}{2} \delta_t$, ensuring the 90° angle, as is indicated in Fig. 1b.

A third specimen was cracked with a needle and then soaked for 7 days in water of 90°C . The observed COD-profile is shown in Fig. 1b. From this profile, Bando et al. [1] claimed that crack-tip blunting would occur at the tip. For an explanation of their

blunting effect, they discussed a process of dissolution and precipitation, depending on the local curvature.

Very early this conclusion was questioned by Lawn et al. [2]. It was shown by these authors that an evaluation of crack opening displacements via the Irwin parabola results in an impossibly high stress intensity factor which was by a factor of 3-4 larger than the fracture toughness of $K_{Ic}=0.8 \text{ MPa}\sqrt{\text{m}}$. Similar argumentation holds for the other cracks, too.

Lawn et al. [2] evaluated the COD of the crack in Fig. 2A (measured in humid air). They obtained over the distance of 150 nm from the crack tip:

$$K = 2.7 \pm 0.2 \text{ MPa}\sqrt{\text{m}} \quad (1)$$

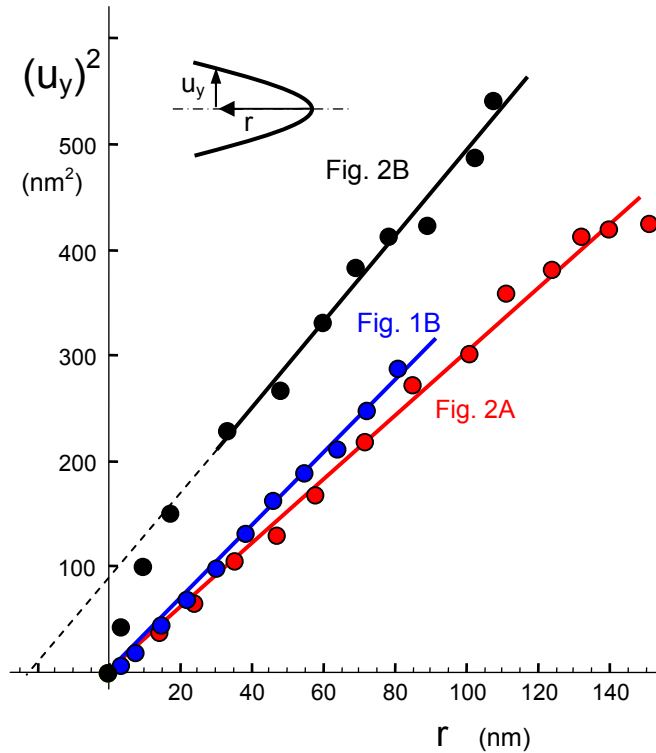


Fig. 2 Crack opening displacements in dependence of the crack-tip distance.

In Fig. 2 the squares of the displacements, $(u_y)^2$, are plotted versus the crack tip distance r for all cracks. Using the near-tip solution for the displacements (counted from the symmetry line to the crack surface), the so-called Irwin parabola,

$$u_y = \sqrt{\frac{8}{\pi} \frac{K}{E}} \sqrt{r} + O(r^{3/2}) \quad (2)$$

suggests linearity of the plots $(u_y)^2=f(r)$ with the slope resulting in K . It should be mentioned that in fracture mechanics the displacements are the difference of the

deformed structure and the undeformed one. From linear regression it results for the tests in air (90% CI in brackets)

$$K_{1B} = 2.65[2.62, 2.68] \text{MPa}\sqrt{\text{m}} \quad (3)$$

$$K_{2A} = 2.48[2.45, 2.51] \text{MPa}\sqrt{\text{m}} \quad (4)$$

and for the water-soaked crack

$$K_{2B} = 2.87[2.69, 3.04] \text{MPa}\sqrt{\text{m}} \quad (5)$$

The stress intensity factors obtained from the far-field displacements are all in good agreement with each other and agree with the result by Lawn et al. [2].

Whereas the fitted straight lines disappear at $r=0$ for profiles Fig. 1B and Fig. 2A, the origin of profile Fig. 2B indicates a shift in the origin to $r=-22$ nm.

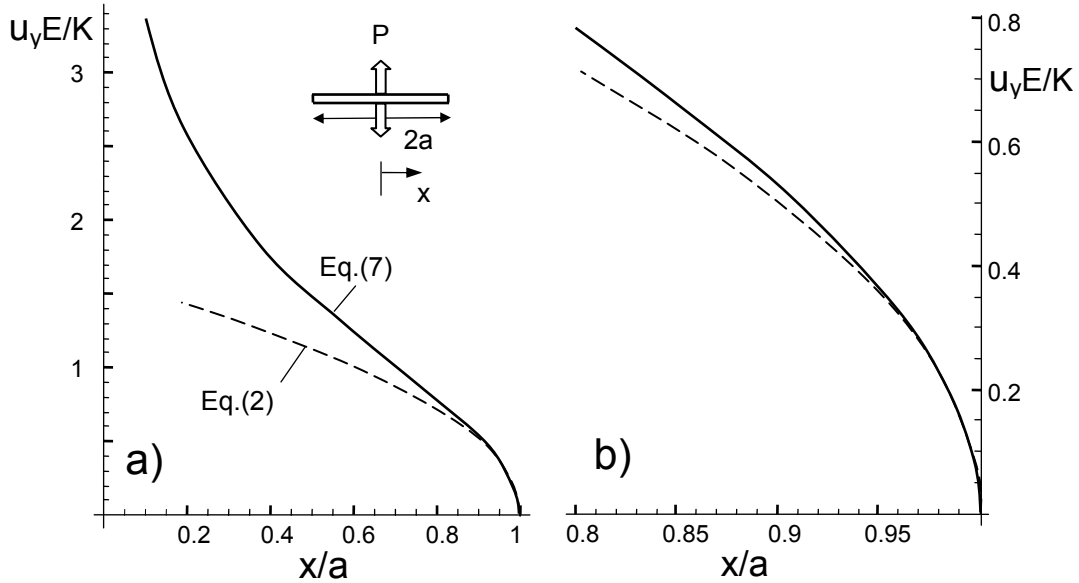


Fig. 3 Crack opening profiles for a crack split by a force P , compared with the near-tip solution eq.(2).

In Fig. 2, the crack-opening displacements (COD), u_y , were evaluated via a near-tip solution, eq.(2). Here this approximation is compared with the full displacement solution for a crack of length $2a$ split by a point-force P in the centre, Fig. 3. For this case, the applied stress intensity factor is

$$K_{appl} = \frac{2P}{\sqrt{\pi a}} \quad (6)$$

where P is the half of the splitting force. The y -displacement normalized on the stress intensity factor reads

$$\frac{u_y}{K_{appl}} = \frac{1}{E'} \sqrt{\frac{a}{\pi}} \left(\ln \left[\frac{x^2}{a^2} \right] - 2 \ln \left[1 + \sqrt{1 - \frac{x^2}{a^2}} \right] \right) \quad (7)$$

This dependency is plotted in Fig. 3a for the whole crack length and in Fig. 3b for the crack-tip region. Deviations between exact solution and the Irwin parabola, eq.(2), are <2% for $0.95 > x/a$ (or $r/a < 0.05$) and about 5% for $x/a = 0.9$ ($r/a = 0.10$). From Fig. 2A in [1] it can be concluded that the crack-length is $a \geq 1.6 \mu\text{m}$. The applied stress intensity factors concluded from the displacements are overestimated by maximum of 5%.

2 Theoretical consequences

2.1 Conclusions on the basis of the J-Integral

At crack tips under externally applied loads, the singular stresses must result in high hydroxyl concentrations and, consequently, high damage followed by a strong stress reduction. As long as a positive crack-tip stress intensity factor exists, $K_{tip} \geq 0$, also stress singularity must exist with $\sigma_{ij} \rightarrow \infty$. The hydroxyl concentration must reach its maximum possible value, S_{max} , with the consequence that the damage must tend to $D \rightarrow 1$ and the Young's modulus must disappear at the tip, $E_D \rightarrow 0$. These consequences make the occurrence of singular stresses and a crack-tip stress intensity factor at least questionable.

The problem will be discussed here by using the path-independence of the J-Integral by Rice [3]. For any time-independent material behaviour the fracture mechanics J-integral can be used as the loading parameter. It simply reads for linear-elastic materials

$$J = \frac{K^2(1-\nu^2)}{E} = G \quad (8)$$

where the right-hand side is also called the energy release rate G . Since the J-integral for any path around the crack tip is a parameter independent of the specially chosen path, its value must be the same for a path Γ far away from the tip (in the bulk) and the path Γ_D directly at the crack tip, i.e. in the damaged region as is illustrated in Fig. 4

$$\frac{K_{appl}^2(1-\nu_0^2)}{E_0} = \frac{K_{tip}^2(1-\nu_D^2)}{E_D} \quad (9)$$

where E_D and ν_D are the elastic properties at the tip affected by water. For $\nu_D \cong \nu_0$

$$K_{tip} \cong K_{appl} \sqrt{\frac{E_D}{E_0}} \quad (10)$$

This equation makes clear why the applied stress intensity factor is much larger than expected from experimental subcritical crack growth data. For the tests by Bando et al.

[1], we assume a final crack velocity of $\approx 10^{-11} - 10^{-10}$ m/s. From the subcritical crack growth curves by Wiederhorn and Bolz [4] the corresponding stress intensity factor in water of 80°C, denoted here as K_{scg} , must result as $K_{scg} \approx 0.3-0.35$ MPa \sqrt{m} (subscript “scg” for subcritical crack growth). The consequence of (1) is that E_D at the crack tip must be strongly reduced by a modulus ratio in the order of $E_D/E_0 \approx 0.01-0.02$.

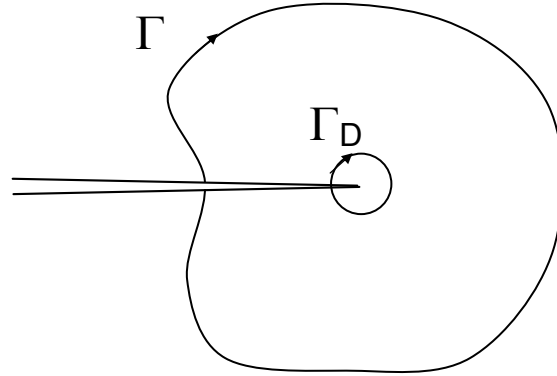


Fig. 4 Two J-integral paths around a crack tip; path Γ far away from the tip reflects the properties of the bulk material, path Γ_D the water-affected and damaged crack-tip region.

2.2 Estimation of crack opening displacements (COD)

In the case of the crack tip located in the damage zone (dashed curve in Fig. 5), the near-tip displacements can be computed analytically.

Introducing (10) into eq.(2) yields

$$u_y = \sqrt{\frac{8}{\pi}} \frac{K_{tip}}{E_D} \sqrt{r} \stackrel{\text{eq.(10)}}{=} \sqrt{\frac{8}{\pi}} \frac{K_{appl}}{E_0} \sqrt{\frac{E_0}{E_D}} \sqrt{r} + O(r) \quad (11)$$

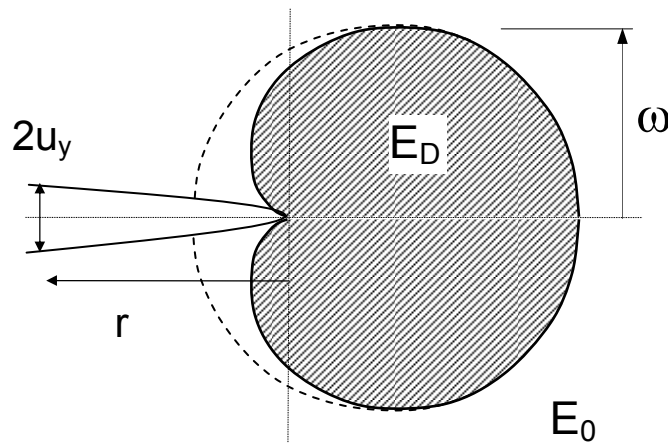


Fig. 5 Crack-tip region under load showing damage zones for “weak swelling” conditions (hatched heart-shaped area) and “strong swelling” (dashed curve).

For the heart-shaped zone (hatched area in Fig. 5), the displacement behaviour is more complicated. In this case, the crack tip belongs as well to the zone of low modulus E_D as to the outer region with Young's module E_0 . Therefore, Finite-Element (FE) calculations were carried out.

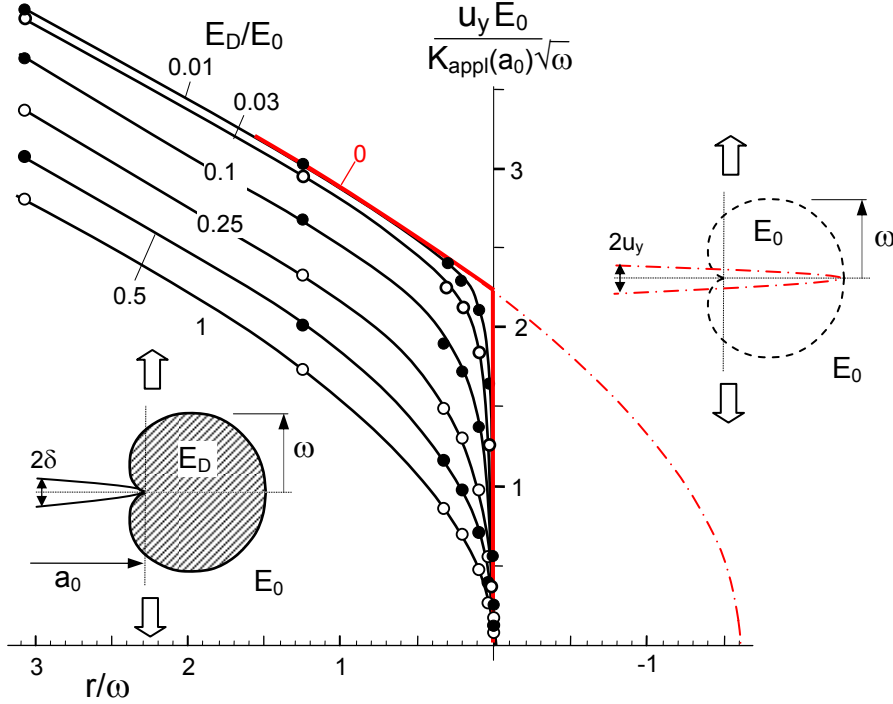


Fig. 6 Normalized near-tip displacements for heart-shaped zones with different Young's modulus (black curves and circles). Solid red curve: Limit case for $E_D/E_0 \rightarrow 0$, dash-dotted curve: Crack of increased length in homogeneous material with $E_D/E_0 = 1$.

The FE-results are plotted in Fig. 6 as the circles. Especially for $r/\omega < 0.3$ the displacements for small Young's modulus are strongly increased. For $r/\omega > 1$ the further increase of COD is the same independent on the module E_D and the curves all appear to be parallel. The red dash-dotted curve represents the limit case of $E_D/E_0 \rightarrow 0$ and an effective crack length that is increased by an amount of $\Delta a = 8/\sqrt{(27)} \omega \approx 1.54 \omega$. From Fig. 6 it is obvious that this limit is sufficiently fulfilled for $E_D/E_0 < 0.03$. For $E_D/E_0 \rightarrow 0$ the limit solution reads

$$u_y = \sqrt{\frac{8}{\pi}} \frac{K_{appl}}{E_0} \sqrt{r + \Delta a} \cong \sqrt{\frac{8}{\pi}} \frac{K_{appl}}{E_0} \sqrt{r + 1.54 \omega} \quad (12)$$

The near-tip behaviour in Fig. 6 leads the observer to believe that “crack-tip blunting” would occur. It should be noted that the COD-problem can also be handled by adopting the models of Elastic-Plastic Fracture Mechanics (EPFM) on Damage.

3 Limit case estimation of zone sizes

The CODs in the near-tip region are somewhat blurred. There are several contours visible in the original image (Fig. 2B in [1]), indicated in Fig. 7. We believe that the thick contour represents the physical crack. The dashed curve shows a zone that extends over a distance of about $L=55\text{nm}$. A further shadowy recognizable contour is introduced in Fig. 7 by the dotted line. Under the assumption that this line might show the damaged zone, a zone length of $L>75\text{nm}$ would result, second column in Table 1. For the height of the zone according to Fig. 5 we first assume that the heart-shaped zones may show the same height as the damaged zones visible on Fig. B2 of [1]. This gives the values of 8.5 nm for the inner and 18 nm for the outer zone in the third column of Table 1. These zone heights must of course underestimate the damage effect because they take into account only the regions near the tip.

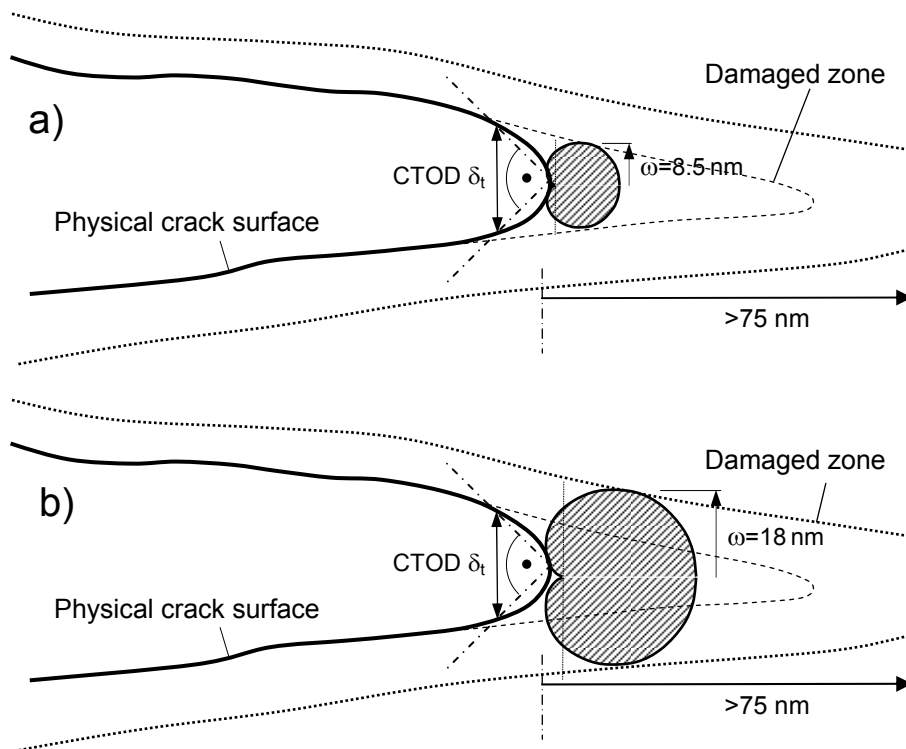


Fig. 7 Zone dimensions visible in the image B2 for the soaked specimen by Bando et al. [1], a) zone height identified as the height of the inner contour, b) zone height given by the height of the outer contour.

Limit case	L	Zone height ω	r/ω	δ_t	Measured δ_t
Lower	55 nm	8.5 nm	1.29	19.3 nm	22 nm
Lower	>75 nm	18 nm	0.61	24.4 nm	“

Table 1 Zone dimensions and evaluation of COD for the heart-shaped zones in Fig. 7.

Since the FE-computations were carried out for a heart-shaped zone, we first will estimate the zone height, ω . For this purpose we compute that heart-shaped zone that shows an identical area with the observed damage zones. The observed area, taken between the crack tip and the right zone ends is compiled in Table 2.

The shape of the zone is in polar coordinates, $r(\varphi)$, given by

$$r(\varphi) = \frac{8}{3\sqrt{3}} \omega \cos^2(\varphi/2) \quad (13)$$

with the polar coordinates defined in Fig. 8. The zone area A is

$$A = \frac{8}{9} \omega^2 \pi \quad (14)$$

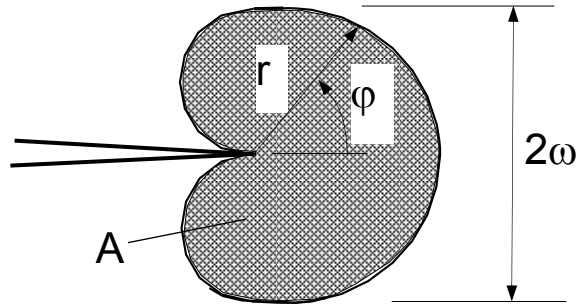


Fig. 8 Heart-shaped damage-zone ahead of a crack tip.

The second column in Table 2 shows the areas for the two assumptions. The area-equivalent zone heights ω for the two possible damaged zones are compiled in Table 2, column 3. Since the CTOD is reached in the distance $r = \delta_t/2 = 11$ nm, the ratio r/ω is known, column 4 in Table 2. These zone heights must of course overestimate the damage effect because they give area-parts in far distance from the tip the same weight as the near-tip region.

Limit case	Area of zone contours	Zone height ω	r/ω	δ_t	Measured δ_t
Upper	720 nm ²	16.05 nm	0.685	23.5 nm	22 nm
Upper	>2500 nm ²	>29.9 nm	<0.375	28.6 nm	22 nm

Table 2 Zone areas for the crack in Fig. 9 (red hatched regions).

In total it can be concluded that the limit case predictions in Tables 1 and 2 agree very well with the measured CTOD.

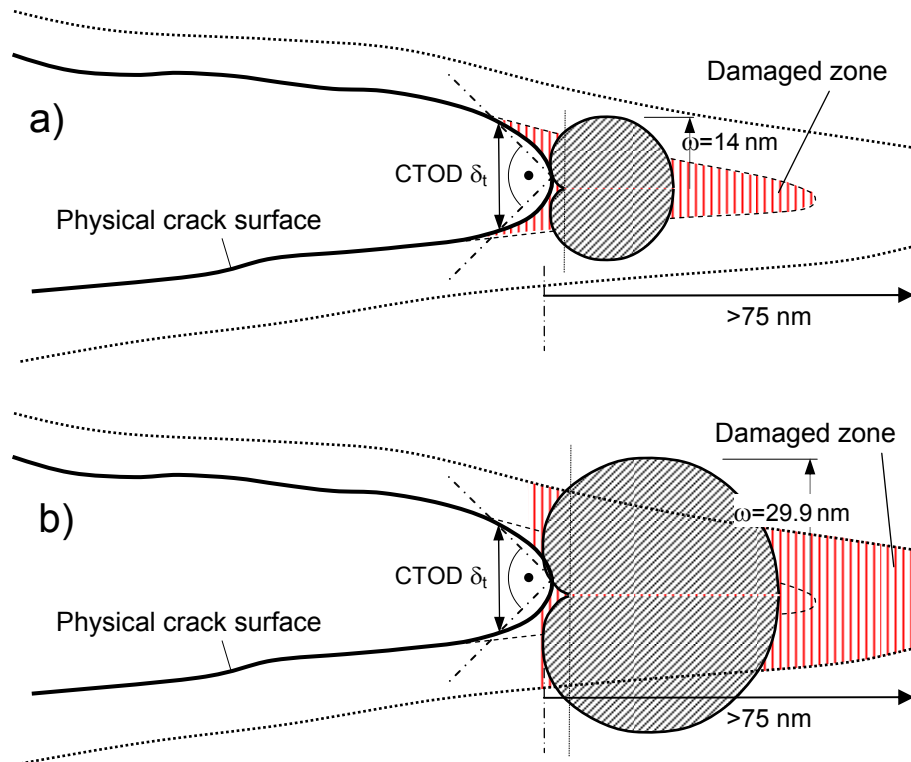


Fig. 9 Zone heights of heart-shaped zones showing the same areas as the observed zones (red hatched regions).

References

- 1 Y. Bando, S. Ito, M. Tomozawa, Direct Observation of Crack Tip Geometry of SiO₂ Glass by High-Resolution Electron Microscopy, *J. Am. Ceram. Soc.*, **67** (1984), C36 C37.
- 2 B.R. Lawn, D.B. Marshall, A.H. Heuer, Comment on "Direct observation of crack tip geometry of SiO₂ glass by high-resolution electron microscopy", *J. Am. Ceram. Soc.* **67**(1984), C253.
- 3 Rice, J.R., A path independent integral and the approximate analysis of strain concentration by notches and cracks, *Trans. ASME, J. Appl. Mech.* (1986), 379-386.
- 4 S.M. Wiederhorn and L.H. Bolz, Stress Corrosion and Static Fatigue of Glass, *J. Am. Ceram. Soc.* **53**(1970) 543-548.

KIT Scientific Working Papers
ISSN 2194-1629

www.kit.edu